COMITATO NAZIONALE PER L'ENERGIA NUCLEARE
Laboratori Nazionali di Frascati

LNF-74/32(R)
12 Giugno 1974

A. Balzarotti, A. Bianconi, E. Burattini and M. Piacentini:
INSTRUMENTAL ASPECTS OF A SYNCHROTRON RADIATION FACILITY.-

Servizio Documentazione
dei Laboratori Nazionali di Frascati del CNEN
Casella Postale 70 - Frascati (Roma)

Laboratori Nazionali di Frascati del CNEN
Servizio Documentazione

LNF-74/32(R)
12 Giugno 1974

A. Balzarotti[x], A. Bianconi[x], E. Burattini[x,+] and M. Piacentini[x,+]: INSTRUMENTAL ASPECTS OF A SYNCHROTRON RADIATION FACILITY[*].

ABSTRACT -

The technical problems encountered in the design of an experimental facility for synchrotron radiation are described. Certain aspects discussed in this paper are often overlooked or not adequately treated in the literature. The optical properties of some focusing mirrors are also illustrated in detail and the solutions adopted at the Frascati's facility are thorougly discussed.

INTRODUCTION -

The radiation emitted by the electrons accelerated in high-energy circular machines causes a costly loss of power and sets the upper limit to the energy of such machines. On the other hand this radiation provided a source advantageous to spectroscopy from the visible to the x-ray region. This spectral range can be covered in laboratory by means of different kinds of lamps, which provide either line spectra and/or continuous spectra. However, the advantages offered by the synchrotron radiation are beyond any discussion:

i) it is emitted whenever the electrons are accelerated in the machine;
ii) its spectrum is continuous over a wide spectral range;
iii) it is highly polarized;
iv) it is much more intense than any other available vuv[1] source.

Because of these peculiarities, the synchrotron radiation is largely utilized in several laboratories for spectroscopic studies of the properties of atoms, molecules and solids[2÷4].

In this paper we review the technical problems encountered in the design of an experimental facility for synchrotron radiation. Some points discussed in the following sections are dealt with in greater detail in other papers or textbooks[5÷8]; however, certain aspects are mentioned but not discussed thoroughly.

Section I deals with the properties of the source. After a brief description of the features of the synchrotron radiation, the dimensions of the source are considered. Section II deals with the pipe connec-

---

(x) - Istituto di Fisica "G. Marconi" dell'Università di Roma.
(+) - Also Fellows of the Consiglio Nazionale delle Ricerche, Sezione di Roma, Roma.
(*) - Research sponsored by CNR as part of the program of the Gruppo Nazionale Struttura della Materia and by the Laboratori Nazionali del CNEN, Frascati.

ting the synchrotron doughnut to the experimental area. In Section III the optical apparatus is discussed and in Section IV the properties of some focusing mirrors are analyzed. Finally the problems of data acquisition and processing are discussed in Section V.

1. - THE SOURCE -

1.1. - The synchrotron radiation. -

The main features of the radiation emitted by relativistically accelerated electrons have been extensively studied both theoretically[9, 10] and experimentally[11, 12]. The characteristic of the radiation emitted by the Frascati synchrotron have been studied experimentally by Missoni and Ruggiero[13], while Balzarotti et al.[14, 15] have measured its spectral distribution.

All the properties of the synchrotron radiation can be derived from the equation

$$(1) \qquad N(\lambda, \psi, E) = \frac{9}{8\pi^2}\frac{e^2}{h}\frac{1}{R^2}(\lambda_c/\lambda)^3\left(\frac{E}{m_o c^2}\right)^5 (1+x^2)^2 \left[K^2_{2/3}(\xi) + \frac{x^2}{1+x^2} K^2_{1/3}(\xi)\right],$$

which gives the number N of photons emitted per sec., per Å and per radiant at the wavelength λ and at the azimuthal angle ψ by an electron of energy E. R is the instantaneous radius of curvature of the electron orbit; $\lambda_c = 5.59\ R(m)/E^3(GeV)$ is a characteristic parameter whose meaning will be discussed below; x and ξ are shorthands for $x = E\psi/m_o c^2$ and $\xi = (\lambda_c/2\lambda)(1+x^2)^{3/2}$; $K_{2/3}$ and $K_{1/3}$ are modified Bessel functions of the second kind of order 2/3 and 1/3 respectively; e, $m_o c^2$ and h have the usual meaning of electron charge, electron rest energy and Planck constant.

a) Angular distribution. -

In the electron frame the radiation is emitted according to the classical dipole pattern. Such a pattern is distorted in the laboratory frame, due to the relativistic transformation of the angles. The light appears to be confined to a narrow cone of aperture $\chi = m_o c^2/E$ pointing in the direction of the particle velocity. Due to the circular motion of the electron, this cone sweeps the observation area, so that one actually observes a horizontal strip of light. From eq. (1) we have calculated the angular distribution of the synchrotron radiation emitted by the Frascati machine in the case of monoenergetic electrons of 1 GeV for different wavelengths and the result is shown in Fig. 1. We note that the emitted intensity drops abruptly at an angle ψ_c defined as the angle at which the intensity is 1/10 of its maximum values. ψ_c is wavelength dependent and increases with increasing wavelength, approaching the value χ near λ_c.

b) Spectral distribution. -

From the observation area, the radiation emitted from the elctronsynchrotron appears as a light pulse of duration $t = (2R/c)(m_o c^2/E)$, corresponding to the time required by the electron to move along an arc 2χ. In the laboratory frame the pulse duration is contracted to the value $t' = (2R/c)(m_o c^2/E)^3$ whose Fourier spectrum will roughly contain all frequencies up to $\omega_c = 1/t'$. The corresponding wavelength $\lambda_c = c/\nu_c = 4\pi R(m_o c^2/E)^3$, gives approximately the shortest wavelength of the spectrum. By integrating eq. (1) over all angles ψ, one obtains the spectral distribution $N(\lambda, E)$ of the synchrotron radiation. The asymptotic behaviour of the spectral distribution function, obtained on expanding it for $\lambda \ll \lambda_c$, shows that the intensity depends strongly on the electron energy, dropping as $e^{-\lambda_c/\lambda}$, so that λ_c has the meaning of a cutoff wavelngth. On the contrary, for $\lambda \gg \lambda_c$, the spectrum does not depend on the electron energy, decresing smoothly as $\lambda^{-4/3}$. Fig. 2 shows $N(\lambda, E)$ calculated for monoenergetic electrons of different energies orbiting in the Frascati synchrotron. The wavelength λ_M at which the maximum of the spectrum occurs, is given by $\lambda_M = 0.7\ \lambda_c$. The power $P(\lambda)$ radiated per Å by each electron is obtained by multiplying $N(\lambda, E)$ by hc/λ; in this case $\lambda_M = 0.42\ \lambda_c$. $N(\lambda, E)$ multiplied by λ^2/hc gives the spectral distribution $N(\hbar\omega)$ in terms of number of photons emitted per sec, per electron and per unit energy bandwidth. Fig. 3 shows all these functions for monoenergetic electrons of 1 GeV orbiting in the Frascati's synchrotron.

c) Polarization. -

The synchrotron radiation is elliptically polarized to a large degree. The two terms in the square brackets of eq. (1) give the intensities $N_{\parallel}$ and $N_{\perp}$ of the two components of the polarization with the elec

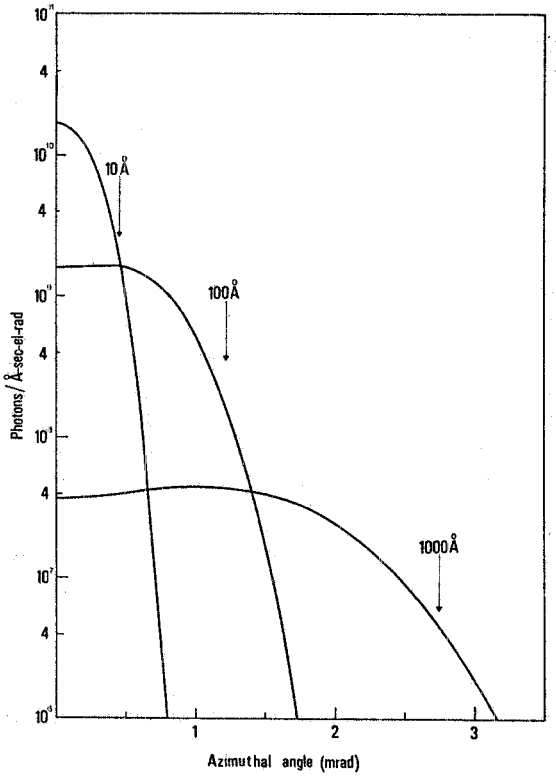

FIG. 1 - Angular distribution of the radiation emitted at different wavelengths by the 1 GeV electrons orbiting in the Frascati electronsynchrotron.

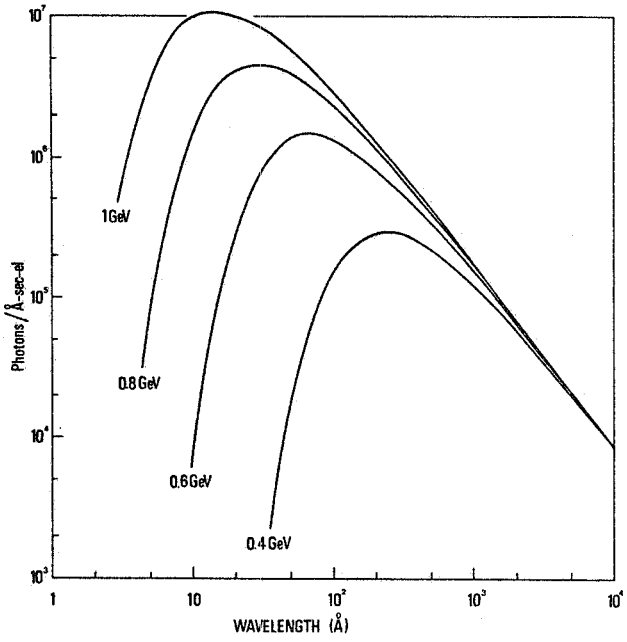

FIG. 2 - Spectral distributions of the radiation emitted by relativistic electrons of different energies orbiting in the Frascati electronsynchrotron.

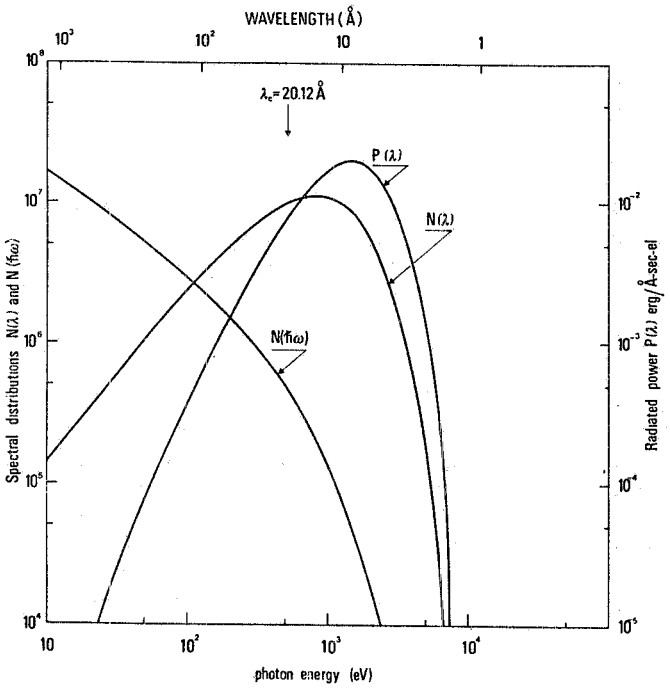

FIG. 3 - Spectral distribution of the radiation emitted by 1 GeV electrons orbiting in the Frascati electronsynchrotron. $N(\hbar\omega)$: number of photons emitted per electron, per second and per unit energy bandwidth. $N(\lambda)$: number of photons emitted per electron, per second and per unit wavelength bandwidth. $P(\lambda)$: power emitted per electron and per unit wavelength bandwidth.

tric field vibrating parallel and perpendicular to the electron orbit plane, respectively. Their angular dependence at three different wavelengths is shown in Fig. 4a. The ratio $N_\perp / N_{//} = [x^2/(1+x^2)]\ (K_{1/3}/K_{2/3})^2$ depends strongly on the azimuthal angle ψ, as shown in Fig. 4b, vanishing in the orbit plane (in which case the radiation is linearly polarized), and approaching 1 at the cone edge ψ_c. If the radiation is collected behind a slit subtending a symmetrical angle ψ_{obs} with respect to the orbit plane, we can define the degree of polarization $\mathcal{P}$ of the collected radiation by means of the equation

$$\mathcal{P} = \frac{I_{//}(\lambda, E) - I_\perp(\lambda, E)}{I_{//}(\lambda, E) + I_\perp(\lambda, E)} \tag{2}$$

where $I_{//,\perp}(\lambda, E) = 2\int_0^{\psi_{obs}} N_{//,\perp}(\lambda, \psi, E)\, d\psi$ represents the whole amount of radiation polarized parallel (perpendicular) to the orbit plane passing through the slit. The degree of polarization $\mathcal{P}$, shown in Fig. 4c, depends on the ratio ψ_{obs}/ψ_c. If ψ_{obs}/ψ_c is small, as in the case of long wavelengths, the degree of polarization is almost 1, meaning that the condition of observation in the orbit plane is nearly satisfied. At short wavelengths, the cone aperture ψ_c is comparable or even smaller than the observation angle and the degree of polarization decreases. Such a behaviour is represented in Fig. 5, where the degree of polarization of the radiation collected within an angle of observation of 0.5 mrad is shown. The curve shows a smooth decrease for decreasing wavelengths except below λ_c, where the intensity of the perpendicular component drops faster than that of the parallel component.

1.2. - The radiation emitted by the electronsynchrotrons. -

Since in electronsynchrotrons the electrons are accelerated from their injection energy E_o up to a maximum energy E_M, the radiation is emitted only during the acceleration cycle, so that it appears in form of light pulses. The spectral distribution obviously changes continuously with electron energy during each pulse, the width of which depends on the wavelength. Infact each wavelength λ is emitted only when the energy of the electrons is sufficiently large, say larger than the energy E_M at which $\lambda_c(E_M)/\lambda \simeq 10$. Fig. 6 shows the energy of the electrons accelerated up to 1 GeV in the Frascati electrosynchrotron (a) as well as the number $\tilde{N}(\lambda, E(t))$ of photons emitted per Å at three different wavelengths by 1cm of the orbit[16] during the acceleration cycle (b). We can see that the pulse duration at 10 Å is much shorter than that at 1000 Å, the former beeing emitted only for $E > 0.6$ GeV, the latter for $E > 0.1$ GeV.

The total number $\mathcal{N}_{tot}(\lambda)$ of photons radiated per Å during the time T_1-T_2 is obtained by adding together all the contributions given by the electron at each revolution during T_1-T_2. We can write it in integral form as

$$\mathcal{N}_{tot}(\lambda) = \int_{T_1}^{T_2} \tilde{N}(\lambda, E(t))\, \frac{dt}{\tau},$$

where τ is the period of revolution (dt/τ is the number of revolution in the interval dt during which the electron can be considered monoenergetic). The average number $\langle N \rangle$ of photons emitted per sec, per Å and per electron during T_1-T_2 is the significant quantity to be compared with the spectral distribution for monoenergetic electrons and it is given by

$$\langle N \rangle = \nu \int_{T_1}^{T_2} \tilde{N}(\lambda, E(t))\, \frac{dt}{\tau}, \tag{3}$$

where ν is the repetition frequency. The eq. (3) gives directly the number of photons/sec/el. entering the experimental set-up. If T_1-T_2 is very small, the average spectral distribution $\langle N \rangle$ approaches the distribution for monoenergetic electrons, except for the duty cycle factor $\nu(T_2-T_1)$. Curve (a) of Fig. 7 corresponds to the spectral distribution in the case of monoenergetic electrons of 1 GeV, while curves (b) and (c) give the average distributions for electrons accelerated up to 1 GeV. Curve (b) corresponds to an interval T_1-T_2 = 1 msec near E_M, while in the curve (c) the average has been taken over the full acceleration cycle.

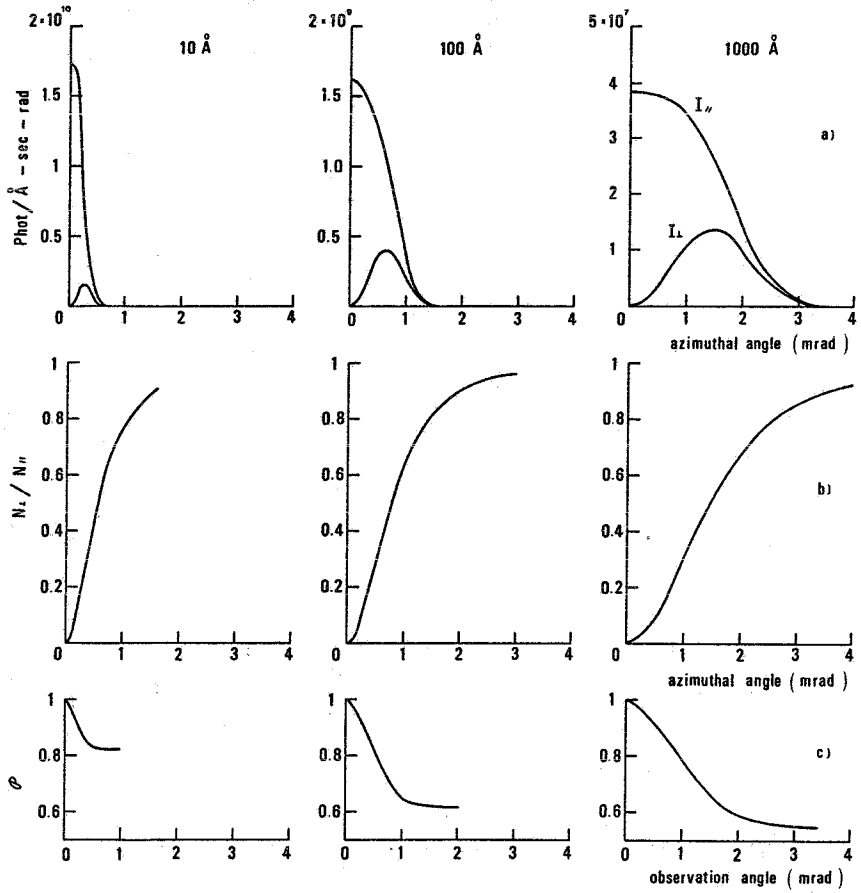

FIG. 4 - Polarization character of the synchrotron radiation:
a) Angular distribution of the two components of polarization emitted at three different wavelengths by 1 GeV electrons orbiting in the Frascati electronsynchrotron. $N_{\parallel}(N_{\perp})$ corresponds to the component with the electric field parallel (perpendicular) to the orbit plane.
b) Ratio $N_{\perp}/N_{\parallel}$ for the distributions shown in a).
c) Degree of polarization $\mathcal{P} = (I_{\parallel} - I_{\perp})/(I_{\parallel} + I_{\perp})$ of the radiation collected by a slit subtending an angle ψ_{obs} with the orbit plane, for the distributions a).

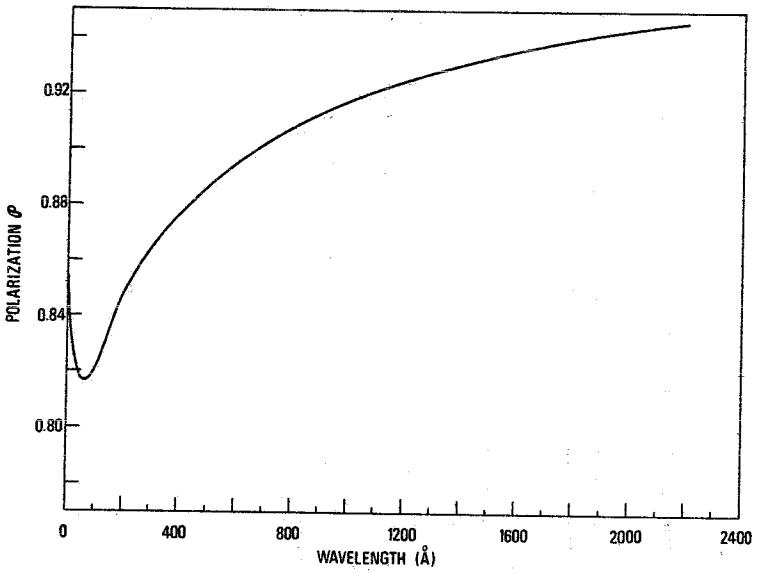

FIG. 5 - Degree of polarization vs wavelength of the radiation emitted by 1 GeV electrons orbiting in the Frascati electronsynchrotron and collected by a slit subtending a 0.5 mrad observation angle symmetric with respect to the orbit plane.

1.3. - Source dimensions. -

So far we have been concerned with the properties of the synchrotron radiation. Let us now consider the characteristics of the source itself.

If the electron orbit is observed through a slit of width w which is set at a distance D from the tangent point, the length L of the observed portion of the orbit is given, to a first approximation, by

$$L = R\delta = \frac{R_w}{D}, \tag{4}$$

where δ is the angle shown in Fig. 8. This result holds for $w/D \ll 1$, a condition which is usually satisfied. Let us derive the exact expression for L. The electron orbit is represented by a circumference $\mathcal{C}$ of radius R and centre at the origin of an x-y frame (Fig. 8). The slit is represented by the segment between the points $S_1 = (D, R)$ and $S_2 = (D, b)$ in the upper half plane $y > 0$. We have to find the angle δ between the two tangents T_1 and T_2 to $\mathcal{C}$ passing through S_1 and S_2. If $P = (x_o, y_o)$ is the point of tangency of T_2 on $\mathcal{C}$, we can write the system of equations:

$$\begin{aligned} y_o &= m\,x_o + c && P \in T_2 \\ b &= mD + c && S_2 \in T_2 \\ y_o &= (R^2 - x_o^2)^{1/2} && P \in \mathcal{C} \\ m &= -\operatorname{tg}\delta = -\frac{x_o}{y_o} && T_2 \text{ tangent to } \mathcal{C} \end{aligned}$$

The solution of this set of equations in the upper half plane is[17]

$$x_o = \frac{R^2}{b^2 + D^2}\left(D - \frac{b}{R}\left(b^2 + D^2 - R^2\right)^{1/2}\right) \tag{5.1.}$$

$$y_o = \frac{R^2}{b^2 + D^2}\left(b + \frac{D}{R}\left(b^2 + D^2 - R^2\right)^{1/2}\right) \tag{5.2}$$

$$\operatorname{tg}\delta = \frac{D - \frac{b}{R}\left(b^2 + D^2 - R^2\right)^{1/2}}{b + \frac{D}{R}\left(b^2 + D^2 - R^2\right)^{1/2}} \tag{5.3}$$

This result is exact. The enequality $D^2 + b^2 > R^2$ holds when S_2 is external to $\mathcal{C}$ and assures for reality of the solutions.

Let us put $b = R - w$ and expand eq. (5.3) in a power series of $w/D \ll 1$. We have:

$$\operatorname{tg}\delta \cong \frac{w}{D} + \frac{R}{2D}\left(\frac{w}{D}\right)^2 + \ldots\ldots, \tag{6}$$

which coincides with eq. (4) provided that the expansion is limited to first order terms. In the case of Frascati's facility $w \cong 3.5$ cm (internal diameter of the pipe), $D = 700$ cm, $R = 360$ cm, so that $w/D = 5.10^{-3}$ and $L = 1.8$ cm.

So far we have neglected the cone aperture ψ_c. Actually during the electron's motion, the slit is illuminated even if the tangent to the orbit does not enter it, as shown by the shadowed area in Fig. 8. The whole angle to be considered is therefore $\delta' = \delta + 2\psi_c$. In the Frascati's set up this introduces an extra-length $\Delta L \simeq 2R\psi_c = 0.36$ cm. for electrons of 1 GeV. The sagittal length s of the arc is given by

$$s = R\left(1 - \cos\left(\frac{\delta'}{2}\right)\right) \simeq R\,\frac{\delta'^2}{8} = 0.8 \times 10^{-3} \text{ cm}.$$

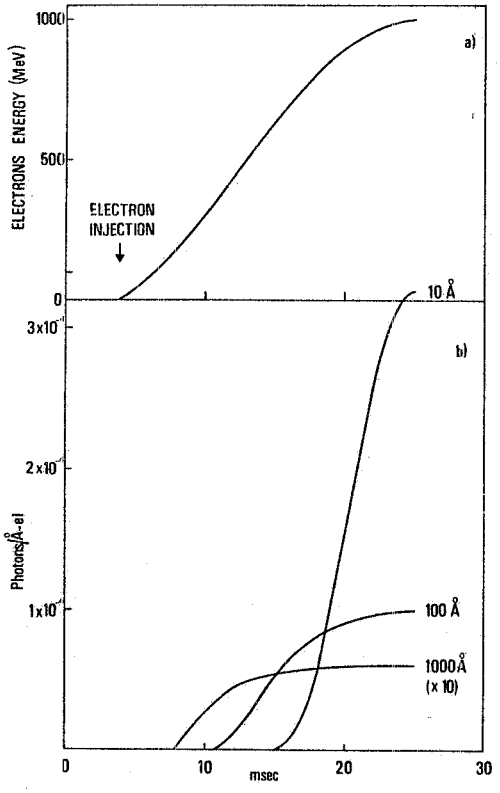

FIG. 6 - a) Energy of the electrons accelerated up to 1 GeV in the Frascati electronsynchrotron vs time.
b) Intensity of the radiation emitted by an electron travelling 1 cm of the orbit during the acceleration time.

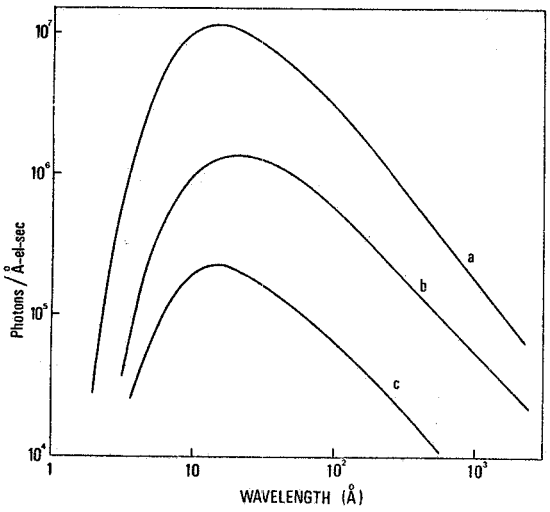

FIG. 7 - a) Spectral distribution of the radiation emitted by electrons orbiting in the Frascati electronsynchrotron in the case of monoenergetic electrons of 1 GeV.
b) Distribution averaged over 1 msec.
c) Distribution averaged over 20 msec.

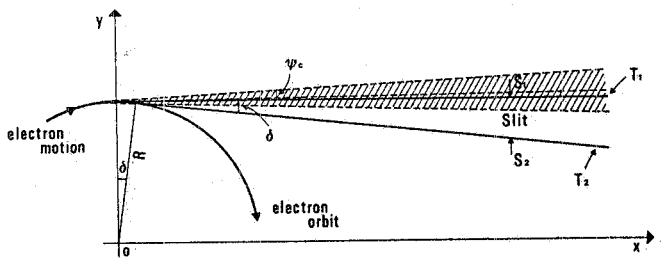

FIG. 8 - Schematic representation of the electron orbit and of the slit illuminated during the electron motion.

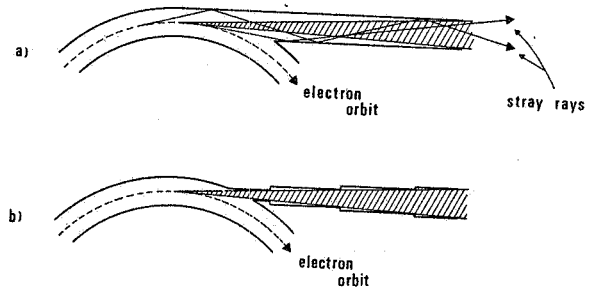

FIG. 9 - a) Scheme of the pipe connecting the synchrotron doughnut to the experimental area, showing the origin of the stray light.
b) Scheme of a pipe of increasing diameter to avoid stray light.

We can see that the dimensions of the radiation source are so small that it can be well approximated by a point source. In most machines the electron beam sizes are larger and one has to take into account its intrinsic dimensions, particularly when the vertical distribution is concerned.

2. - THE PIPE -

A vacuum pipe connecting the synchrotron doughnut to the experimental layout is required because the far ultraviolet (FUV) radiation is completely absorbed by few millimeters of air. It is practically convenient to divide the pipe in sections so that insertion of new devices is easily performed by changing only one section. The diameter of the tubing may increase going farther from the doughnut in order to decrease the amount of stray light reaching the experimental area. In our opinion, the stray light is the main problem connected with the design of the vacuum pipe and we will discuss it briefly.

The radiation emitted by the electrons during their motion hits the walls of the pipe at nearly grazing incidence and is reflected almost totally. (Fig. 9a). Because of the roughness of the walls the radiation is scattered in all directions giving rise to a large amount of stray light at the end of the pipe. To avoid stray light reaching the experimental apparatus, the diameter of each section must be calculated so as to shield all the radiation laying outside the cone filling the observation area. (Fig. 9b). Alternatively one can insert shields of different aperture along the pipe. If w x h are the dimensions of the observation area distance D away from the orbit and D_i is the distance of the shield i from the tangent point, the shield aperture should be w D_i/D large and hD_i/D high.

In some Laboratories the health service allows researches to operate near the equipment when the electrons are accelerated, provided that a lead shield is inserted along the pipe to avoid the radiation. In such a cases a removable shield of proper dimensions must be foreseen in designing the pipe.

Another problem that must be considered is the optical alignment of the devices, which cannot be accomplished by looking at the path of the synchrotron radiation directly.

A laser beam is necessary for this purpose. In some facilities the laser is aligned along the tangent line to the orbit at the opposite side of the synchrotron doughnut, namely in the backward direction of the electron motion. This system can be operated only when the electrons are not accelerated, since other wise the operations near the experimental area are allowed only with the lead shield inserted in the beam. Such difficulties can be avoided setting the laser after the lead shield at 90° with respect to the light direction as shown in Fig. 10. The alignment can be checked with synchrotron radiation by means of either a closed television circuit or photografic plates[18].

3. - THE OPTICAL EQUIPMENT -

3.1. - General considerations. -

The optical system must be designed without lenses and windows as the absorption coefficient of all materials is very large (10^4 - 10^6 cm^{-1}) beyond the LiF absorption edge (~1100 Å). Only in special cases small windows can be constructed using thin films (few hundreths Å thick) of proper materials, such as formvar or gold, supported by very thin meshes of high transparency[7]. The reflectivity is also very low in the FUV. Only noble metals have a reflectivity as high as a few percent down to 400 Å at normal incidence[19-21]. At angles of incidence larger than the critical angle ϑ_c = arcsin (n) the phenomenon of total reflection takes place and the reflectivity tends to 1 in the limit of no absorption.

Since the optical elements work in reflection, some care must be taken in designing the optical equipment for synchrotron radiation. As discussed in Sect. I, the synchrotron radiation is elliptically polarized with the major axis of the ellipse lying in the plane of the electron orbit. Since p-polarized light is reflected less than s-polarized light at every angle of incidence, the incidence plane of any reflecting surface should be perpendicular to the orbit plane. This arrangement is sometimes referred as a "vertical" mounting in order to distinguish it from the more common "horizonthal" mounting having the plane of incidence parallel to the orbit plane (Fig. 11).

Let us consider, as an example, a gold mirror reflecting radiation of 400 Å at an angle of incidence $\vartheta = 80°$. At this wavelength the optical constants of gold are n = 0.9 and k = 0.6[19], giving R_p=0.49 and R_s = 0.71. From fig. 5 the degree of polarization of the synchrotron radiation at 400 Å is about 0.88.

If the incident intensity is normalized to 1, we obtain $I_R = 0.5$ in the horizontal mounting and $I_R = 0.7$ in the vertical mounting. The corresponding degrees of polarization are 0.83 and 0.91, respectively, showing that the vertical disposition increases the polarization degree of the radiation.

3.2. - Monochromators. -

In this note we will not discuss in detail the types of monochromators for FUV since this subject is treated in several specialized textbooks[7, 8]. The dispersive element is the reflecting grating mounted at near normal incidence in the case of long wavelengths and at grazing incidence for shorts wavelengths.

Commercial near-normal incidence monochromators have a horizontal mounting with both entrance and exit slits fixed. The grating is concave to focus the radiation and the scanning is performed by rotating and translating the grating. Gratings are blazed to increase their efficiency and are generally coated with Al or Al+MgF_2 to improve the efficiency at $\lambda > 1100$ Å[21], or with Au or Pt to increase the efficiency at $\lambda < 1100$ Å[19, 20] (Fig. 12). These monochromators have very low astigmatism, so they can provide very high resolution. To fit the needs of synchrotron radiation, special normal incidence monochromators have been designed in some Laboratories. The point source, corresponding to the electron beam, is focused by a concave grating directly on the exit slit, so that the entrance slit is not required anymore. The shortest wavelengths scanned is about 400 Å, since below this the reflectivity of the material coating the grating drops rapidly to zero.

Commercial grazing incidence monochromators work in the simplest mounting which assures perfect focusing over the whole spectral range: the concave grating, the entrance and exit slits are on the Rowland circle and the scanning is performed moving the exit slit along the circle. Both horizontal and vertical mountings are found in commercial instruments. The entrance slit is movable with respect to the grating in order to set different angles of incidence. However the astigmatism increases at grazing incidence putting severe limits on the use of the instrument at long wavelengths. The major difficulties encountered in the commercial monochromators, when used in connection with synchrotron radiation, are the presence of higher spectral orders of diffraction and the moving exit slit. To overcome these difficulties, more complicate intruments have been developed in several laboratories[22] with two or three reflecting elements.

3.3. - Grating illumination. -

The synchrotron radiation can be approximately considered as formed by parallel rays. The illuminated area of the grating is therefore the image of the entrance slit of the monochromator. When using narrow slits to achieve high resolution, this fact seriously affects the instrument resolution which is proportional to the number of illuminated rulings. This means that, with slit aperture of 100 μ, only 120 grooves of a 1200 line/mm grating are illuminated at normal incidence. It becomes necessary therefore to use a focusing mirror to image a large portion of the incident beam on the entrance slit of the monochromator with such an angular divergence that all the ruled area is illuminated. The features of these focusing mirrors will be discussed in the next section. Here we want only to point out that some care must be taken in choosing the proper angle of incidence in order not to eliminate the portion of the shortest wavelengths of the spectrum.

3.4. - Filters. -

The spectral range covered by the synchrotron radiation is so large that suitable filters are required to avoid higher orders of diffraction at the exit slit of the monochromator. The problem is serious in the case of grazing incidence instruments, for which the ratio between second and first order intensities is large and, for some gratings, even larger than 1[23].

Thin films of materials having their absorption edges in the desired range are used to filtering out shorter wavelengths. Since at the absorption edge the absorption coefficient increases steeply by a factor of ten or more, there is a real cutoff in the transmitted radiation of higher energy. Fig. 13 shows the transmittance of several materials in the FUV[24-26]. However, the use of thin films as filters is limited by practical problems. Some films need to be supported by substrates which must have a flat and high transmittance in the desired spectral range. Organic substances, such as formvar, are very good for this purpose except in the soft x-rays region where the K absorption of some of their main constituents, like carbon, oxygen and nitrogen, occur at 43.77, 23.37 and 31.05 Å respectively. Moreover even good quality films obtained by evaporation have often some holes which give a background of stray light.

Mirrors reflecting at grazing incidence provide a second kind of filter. Infact at very short wavelenghts the index of refraction n of the medium is well described by the free electron equation $n^2 = 1 - \lambda^2/\lambda_p^2$,

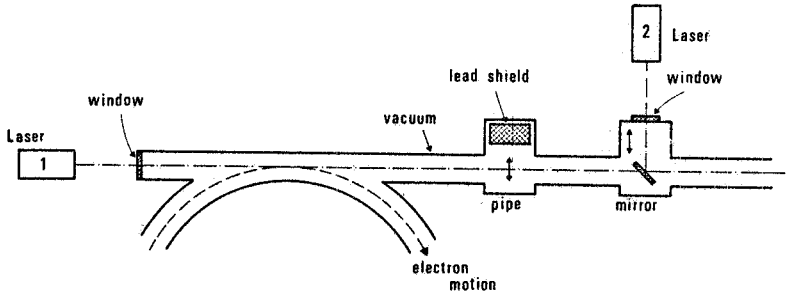

FIG. 10 - Diagram showing two possible positions of a laser for optical alignements. Position 1 correspond to a laser aligned along the pipe in the backward direction of motion of the electrons. Position 2 corresponds to the lateral alignement of the laser at 90° with respect to the pipe.

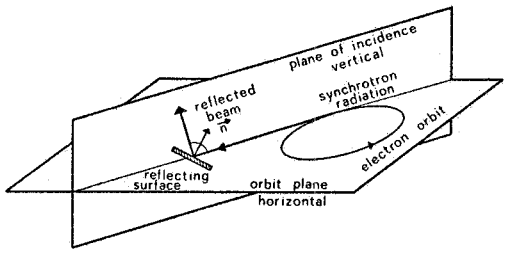

FIG. 11 - Diagram showing the "vertical" mounting to match the polarization character of the synchrotron radiation.

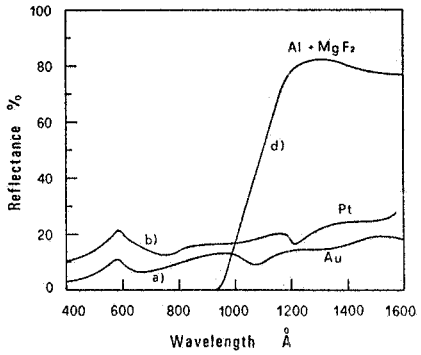

FIG. 12 - Efficiency of several materials used as coatings for gratings. Au, Ref. (19); Pt, Ref. (20); Al, Ref. (21); Al+MgF_2, Ref. (21).

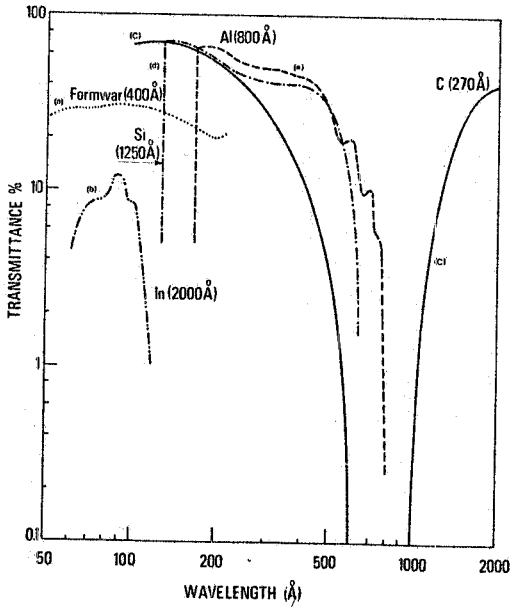

FIG. 13 - Transmittivity of several materials in the FUV.
a) Formvar, Ref. (15);
b) In, (unpublished data, A. Balzarotti et al.);
c) C, Ref. (26);
d) Si, Ref. (24);
e) Al, Ref. (24).

where λ_p is the wavelength corresponding to the plasma frequency of the free electrons of the reflecting material. By introducing the grazing incidence angle $\theta = \pi/2 - \theta$, we can write from the equation $\sin\theta_c = n$, the following relation for the dependence of the critical angle θ_c on the wavelength:

$$\theta_c = \lambda / \lambda_p \,, \tag{7}$$

which is valid in the limit $\lambda \ll \lambda_p$. The eq. 7 shows that only wavelengths longer than the critical wavelength $\lambda_c = \theta_c \lambda_p$ are totally reflected. Fig. 14 shows the reflectivity of the aluminum versus wavelength at different angles of incidence. The full curves have been calculated using the optical constants of aluminum reported by Sasaki[27]. The broken curves are the result obtained by using the free electron index of refraction with $\lambda_p = 381.4$ Å, corresponding to the oscillation of all the 13 electrons of aluminum. The two sets of curves are coincident at very short wavelengths and very large angles; their main difference at longer wavelengths comes from the finite, even if small, value of k which lowers (and gives some structure to) the reflectivity in the region of total reflection.

Similar arguments hold for the gratings. The intensity of the radiation diffracted in the order m has jumps in correspondence to the critical wavelength $\lambda_c^{(0)}$ of the zero order and to the critical wavelength $\lambda_c^{(m)}$ of the order m[28, 29]. The critical wavelength is given in general form by

$$\lambda_c^{(m)} = \frac{\lambda_p^2}{d} \left(-m + \sqrt{m^2 + \frac{2d^2}{\lambda_p^2}(1-\cos\theta)}\right) \tag{8}$$

where d is the grating parameter. For the inside spectrum ($m < 0$) $\lambda_c^{(0)} < \lambda_c^{|m|} < \lambda_c^{|m|+1}$ while for the outside spectrum ($m > 0$) $\lambda_c^{(0)} > \lambda_c^{|m|} > \lambda_c^{|m|+1}$. Then the grating provides to the first order a range of wavelengths free of higher orders, given by $\lambda_c^{(0)} < \lambda < 2\lambda_c^{(0)}$ for the inside spectrum and by $\lambda_c^{(1)} < \lambda < 2\lambda_c^{(2)}$ for the inside spectrum.

The monochromators specially designed to work with synchrotron radiation scan wavelengths through the rotation of the grating (or eventually of a mirror) in such a way as to satisfy the condition of free spectral range. Things are simpler in the case of normal incidence; Si or Te films provide good filters below 600 Å, while LiF and quartz have respectively their absorption edges at 1100 Å and 1800 Å, so that the entire spectral range up to 3000 Å can be covered without overlapping of higher orders by only interchanging such materials.

4. - THE FOCUSING MIRRORS -

The choice of the focusing mirrors depends upon the kind of source one considers. If the experimental set-up is far from the electron orbit, so that the radiation practically consists of parallel rays, a parabolic mirror is required; if the source is considered as a point source, an elliptic mirror has to be preferred. In both cases the manufacturing of these mirrors is difficult and expensive and for practical purposes spherical mirrors also give good imaging.

4.1. - Parabolic mirror. -

The conditions used to calculate a parabolic mirror (Fig. 15) are the following:

a) The angle of incidence θ on the mirror must be larger than a certain value θ_M. This value is chosen either to have a large reflectivity over the entire spectral range or to avoid filtering of the shortest wavelengths.

b) The distance of the illuminated portion of the mirror from the focus must have reasonable values.

The set of equations satisfying the above conditions are obtained in Appendix I, equations A1-4 and A1-5.

Let us now calculate the parameters of a parabolic mirror in front of a near-normal incidence monochromator. In order to get a large reflectivity above 300 Å, we choose $\Theta_M = \pi/2 - \theta_M = 20^\circ$, (see Fig. 14). We also require $\chi = 3^\circ$ in order to fill the whole ruled area of the grating. From eq. A1-4 we

get $x_o/d = 0.766$; $y_o/d = 0.643$; $a/d = 0.117$. From eq. A1-5 we have: $x_1/d = 0.91$; $y_1/d = 0.693$; $\widehat{P_oP_1}/d = 0.152$; $w/d = 0.05$. Choosing $w = 3$ cm, we have $d = 60$ cm and $\widehat{P_oP_1} = 9.1$ cm.

4.2. - Elliptic mirror. -

Let us refer to the Fig. 16, representing the ellipse generating the mirror. The conditions to determine both the parameters of the ellipse and the length of the mirror $\widehat{P_1P_2}$ are the following:

a) The distances of P_1 from the source at F_1 and from the image at F_2 are limited by the dimensions of the system.

b) The grazing angle of incidence should be less than θ_M as for the parabolic mirror.

c) The angle $\delta = \hat{P_1F_1P_2}$, corresponding to the observation angle, is fixed.

d) The angle $\chi = \hat{P_1F_2P_2}$, corresponding to the divergence of the reflected beam, must fulfill the conditions of grating illumination.

The detailed derivation of the equations determining the parameters of the ellipse is given in Appendix II. As an example, we report in Table I the parameters calculated for a real case appropriate to the Frascati facility.

TABLE I - Parameters of the ellipse and of the elliptic mirror. The quantities in the first column refer to the case of the Frascati facility.

	Ellipse parameters	Mirror parameters
$\theta = 20^o$	$u^2 = 0.0466$	$x_1 = 307$ cm
$\chi = 3^o$	$Q = 400$ cm	$y_1 = 81$ cm
$\delta = 4.10^{-3}$ rad.	$f = 391$ cm	$\theta_1 = 18^o\ 37'$
$D = 700$ cm	$q = 85$ cm	$x_2 = 324$ cm
$d = 100$ cm		$y_2 = 47.5$ cm

4.3. - Spherical mirror. -

Since spherical mirrors are easier to built, they are often used instead of elliptical or parabolic mirrors. Spherical mirrors of radius R have the property that each point lying on a circle whose diameter is 2R (Rowland circle) is re-imaged on the same circle, provided that the dimensions of the mirror are much smaller that the radius of curvature of the sphere. This property holds only in the plane of incidence and in this case we speak of "horizontal focus". Actually the image of a point source at the horizontal focus is a vertical line whose dimensions are still minimized at a different point, called the "vertical focus". In the case of a spherical mirror of radius R, the positions of the horizontal and of the vertical foci are given by

$$\text{horizontal focus} \quad \frac{1}{s} + \frac{1}{s_h} = \frac{2}{R\cos\theta}$$

$$\text{vertical focus} \quad \frac{1}{s} + \frac{1}{s_v} = \frac{2\cos\theta}{R} \tag{9}$$

where θ is the angle of incidence, s, s_h and s_v are the distances from the center of the mirror, of the source, of the horizontal focus and of the vertical focus, respectively.

From the above considerations, we see that the image of a point source given by of a spherical mirror is astigmatic. Anyhow, using a toroidal mirror with proper horizontal and vertical radii of curvature, the two foci can be brought into one another. The two radii are calculated setting $s_h = s_v$ in eq. (9).

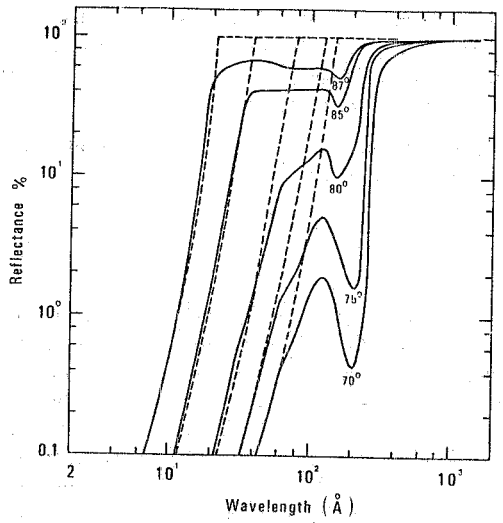

FIG. 14 - Calculated reflectivity of aluminum at different angles of incidence. Full lines: Calculations performed with the optical constants of Ref. (27). Broken lines: Calculations performed using the equation $C = 1 - \lambda^2/\lambda_p^2$.

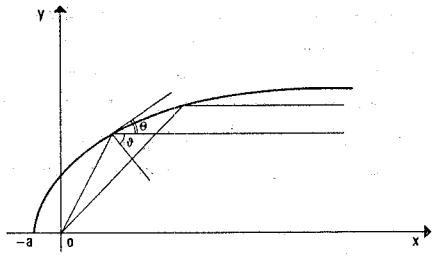

FIG. 15 - Parabolic mirror: the parallel rays, incident from the positive x direction are reflected at grazing incidence in the focus.

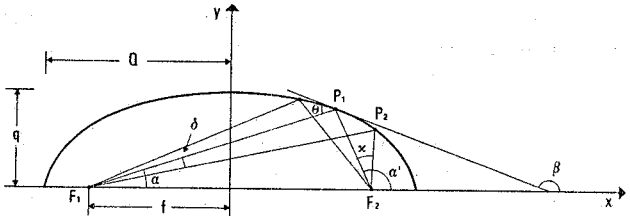

FIG. 16 - Elliptic mirror: the rays, emitted from a focus (electron orbit) are reflected at grazing incidence in the other focus of the ellipse (monochromator's entrance slit).

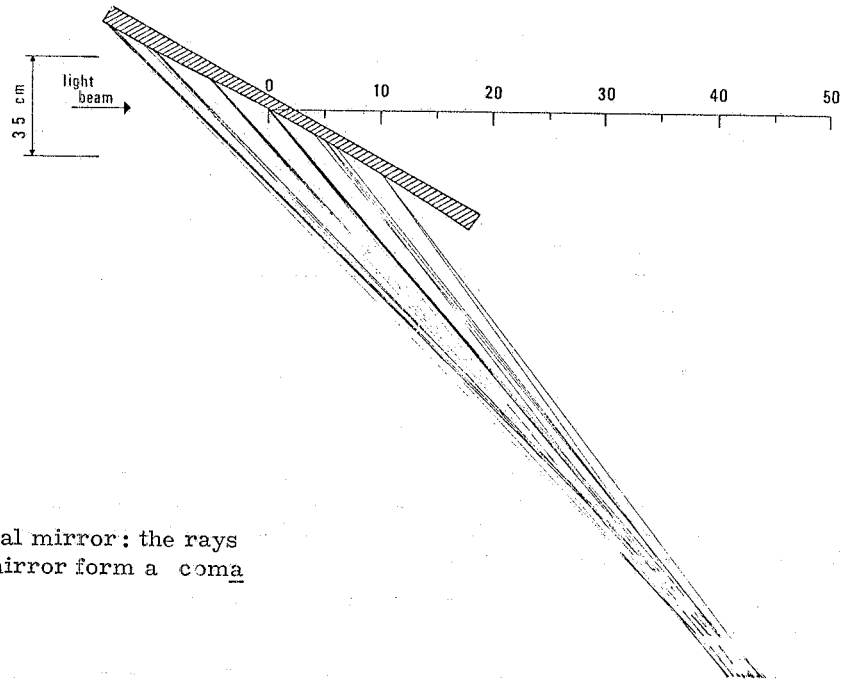

FIG. 17 - Spherical mirror: the rays reflected by the mirror form a comatic image.

At grazing incidence the conditions to obtain a good focus are not satisfied anymore, since mirrors of large dimensions are required. The image becomes comatic. Fig. 17 shows the focusing properties of a spherical mirror of radius R = 380 cm designed at the Frascati facility to focus the synchrotron light on the entrance slit of a Higher & Watts normal-incidence monochromator.

The detailed characteristics of this mirror are described in Appendix III. A photograph showing the mirror and the mechanisms of translation and rotation is presented in Fig. 18.

5. - THE MEASUREMENTS -

The sample chamber for experiments of reflection and transmission[30] is generally attached to the exit slit of the monochromator to avoid radiation damage of the sample exposed to the whole spectrum of the synchrotron radiation or to avoid luminescence induced in the sample by high-energy photons. In the short wavelengths region (below 400 Å), only transmission experiments can be performed, the normal incidence reflectivity being too small to be measured. Since the absorption coefficient of any material may range between 10^4 to 10^6 cm^{-1} in the VUV, thin films, few hundredths Å thick, must be used to have transmission larger than some percent. It is convenient to prepare thin films "in situ" and therefore the sample chamber must contain an evaporation system. This procedure of treating samples avoids surface contamination or chemical changes of the films, provided that an ultra-high vacuum ($< 10^{-9}$ mmHg) is maintained in the chamber. Since commercial instruments usually work in the range of 10^{-6} torr, either a differential pumping between the monochromator and the sample chamber or a window of the type described in Sect. 3.4 are required. Back-streaming of the oil of the diffusion pumps must be absolutely avoided, because its deposition on surfaces exposed to the VUV radiation causes the formation of carbon layers.

The detection of the radiation is achieved with open electron multipliers having tungsten photocatodes, whose spectral response ranges from 5 to 1300 Å[31]. These detectors are also sensitive to charged particles and must work in high vacuum. Care must therefore be taken to shield ion sources, such as vacuum ion gauges, in the sample chamber. From 300 Å up to near ultraviolet, sodium salicylate is commonly used as fluorescent material. Its emission is peaked at 4200 Å, which is coincident with the maximum sensitivity of a photomultiplier with a S11 response.

If the available light levels to be detected are below 10^2 photons per sec, the single photon counting technique must be used to detect the signals. For this purpose channeltron electron multipliers are commonly used since their dark noise is very low, of the order of one pulse per sec. The connection to the amplifier-discriminator must be as short as possible and care must be taken to shield cables in order to avoid pick-ups from radiofrequency sources or from other fast transients.

The analogic processing needs a preamplifier and a voltmeter. To increase the S/N ratio, the radiation is chopped and the signals are integrated with in-phase amplifiers.

Both reflection and transmission measurements require two signals, the intensity of the reflected (transmitted) radiation from the sample and that of the incident radiation. It is very convenient to measure both signals at the same time to avoid errors arising from source fluctuations connected with the different spectral distributions emitted from electron of different energy and from changes in the performance of the optical apparatus. A double beam system is normally employed in this case. If the double beam technique is not used, each signal I and I_o can be normalized to the number of electrons orbiting in the machine. A photomultiplier is inserted along the pipe looking at the synchrotron beam, and a signal proportional to the number N of electrons is obtained

$$I_r = N \int_{\lambda_1}^{\lambda_2} G(\lambda)\mathcal{P}(\lambda)d\lambda \qquad (9)$$

where $\mathcal{P}(\lambda)$ is the spectral distribution function of the synchrotron radiation and $G(\lambda)$ is the efficiency of the system (Photomultiplier, mirror, windows etc.). λ_1 and λ_2 define the wavelength range in which the efficiency of the cathode of the photomultiplier is different from zero. The integral in eq. (9) is a constant depending only on the parameters of the device so that $I_r \propto N$.

All signals can be recorded on chart x-y recorders or, if possible, on magnetic tapes to simplify processing on large computers.

In a synchrotron radiation facility a small on-line computer is a very powerfull tool[32]. The com

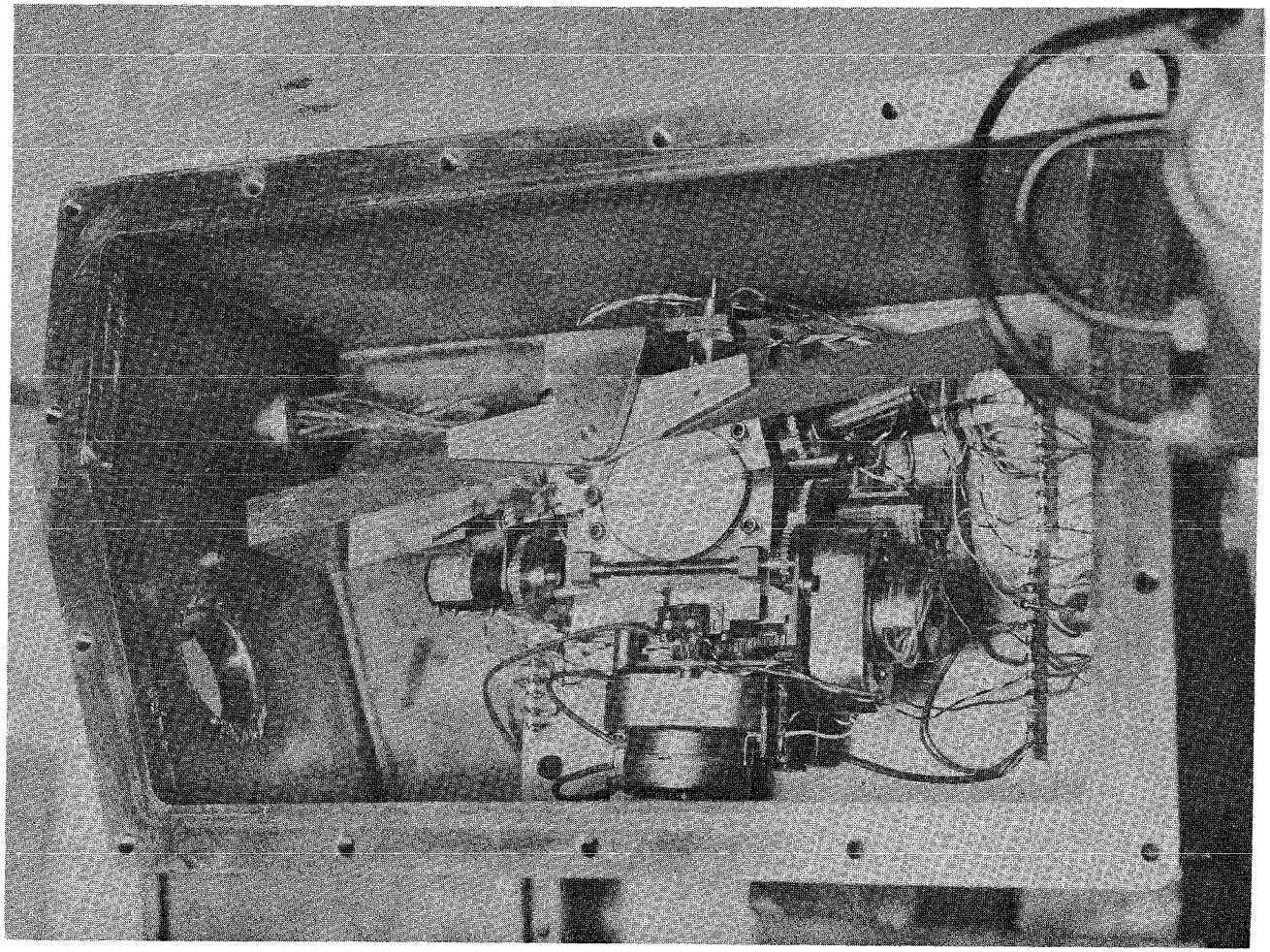

FIG. 18 - Gold-coated spherical mirror of radius R built at the Frascati's facility. Note the x-y mouvements and the rotation mechanism about the z axis.

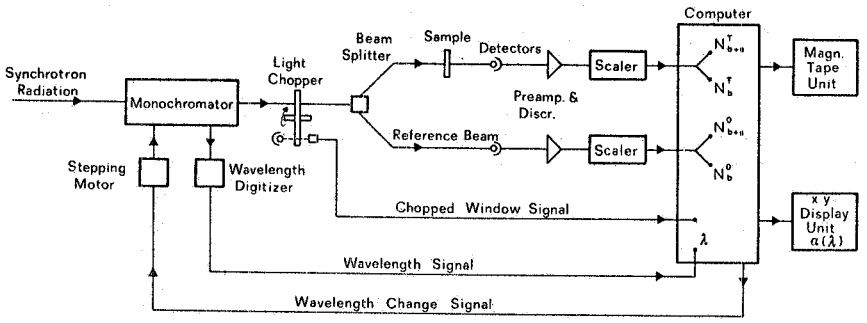

FIG. 19 - Block diagram showing the use of an on-line computer in a transmission experiment.

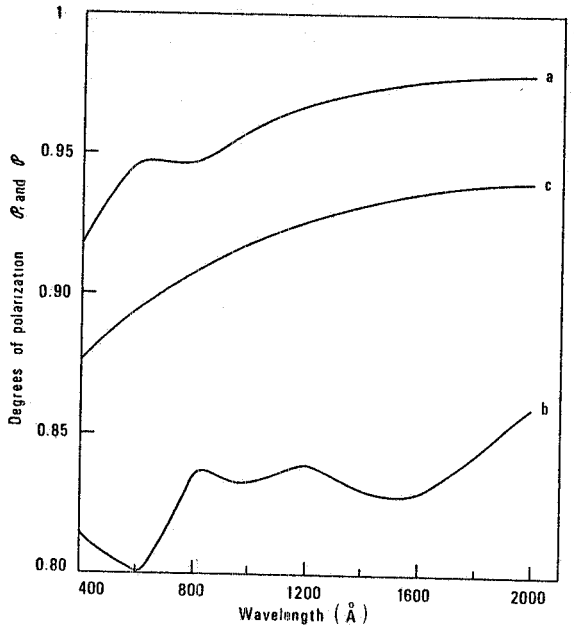

FIG. 20 - Degree of polarization $\mathcal{P}_r$ of the light reflected at $\vartheta = 78^\circ$ from a gold-coated spherical mirror in vertical (a) and horizontal (b) mountings. The degree of polarization $\mathcal{P}$ of the synchrotron light (curve c), taken from Fig. 5, is shown for comparison.

puter can drive the experiment, record and storage signals on magnetic tape, perform preliminary calcu lations and display the results on a plotter, so that the experiment can be followed while it is running. In Fig. 19 a possible block diagram of a transmission experiment with single photon counting detection and computer control is shown.

The radiation of wavelength λ emerging from the exit slit of the monochromator is chopped and splitted in two beams. A beam goes through the sample and is detected by a photomultiplier providing the number of transmitted photons N^T. The other beam goes directly to a second photomultiplier and provides the number of incident photons N^o. Both signals, after the preamplifiers and the discriminators, are fed into two scalers interfaced to the computer, which also receives a pulsed signal from the chopper. The computer can be programmed as follows. When the chopper window is open, the counts corresponding to the signals plus the backgrounds are stored into two channels N^T_{b+s} and N^o_{b+s}. When the chopper window is closed, the counts corresponding to the backgrounds only are stored into two different channels N^T_b and N^o_b. After a preselected number of chopper cycles, the computer stops counting and performs some calculations such as the subtraction of backgrounds from signals $N^{(T,0)}_{b+s} - N^{(T,0)}_b = N^{(T,0)}$, ratio N^T/N^0, computation of statistical errors etc. All these data as well as the wavelength, can be transferred onto a magnetic tape and at the same time the $\log(N^0/N^T)$ can be displayed on a display (or an x-y chart recorder) as a function of the wavelength. Now the computer can command the change of the wavelength sending a preselected number of pulses to a stepping motor connected to the scanning mechanism of the monochromator, and it can start the whole cycle again. In this way the whole spectrum can be scanned automatically, data are stored on a tape for easier use later. Contemporaneously the researcher can follow on the display the experiment while it is running and, if necessary, he can manually change the experimental conditions.

We would like to stress that in a laboratory where a synchrotron radiation facility is developing, the use of a small on-line computer may result also in saving money. Even if the cost of the computer itself and of its peripherals is high, its interfacing to the experiment is not expensive. If several experiments are driven at the same time, the average cost of the electronics per experiment is comparable or even less than that of the standard electronic required by each experiment. Another advantage is the time saved in the analysis of the data after the experiment.

APPENDIX I -

Let us consider the radiation beam emitted from the synchrotron to be parallel to the x axis of an xy frame in the upper positive half plane ($y > 0$). The equation of a parabola having its focus in the origin of the reference frame and its axis along the x axis, is given by (see Fig. 15)

$$y = 2\,(a\,(x + a))^{1/2}, \tag{A1-1}$$

where - a is the abscissa of the vertex. Let us rewrite the equation (A1-1) in a different form, in terms of the grazing angle of incidence θ, corresponding to the angle between the tangent to the parabola and the x axis. The condition $\theta > \theta_M$ becomes $\theta < \theta_M$ (where $\theta_M = \pi/2 - \theta_M$). Tg θ_M is obtained taking the derivative of the eq. (A1-1) at P = (x, y):

$$Tg\,\theta = \left.\frac{dy}{dx}\right|_P = (a/(x+a))^{1/2}, \tag{A1-2}$$

which increases with decreasing the values of x. The point on the parabola corresponding to θ_M is therefore the nearest to the focus and we want that such a distance be d. We can now write the following three equations

$$\begin{aligned} y_o &= 2\,(a(x_o + a))^{1/2} \\ tg\,\theta_M &= (a/\,(x_o + a))^{1/2} \\ x_o^2 + y_o^2 &= d^2 \end{aligned} \tag{A1-3}$$

which allow us to find the parameter a and the coordinates of P_o:

$$x_o/d = \frac{1-tg^2\,\theta_M}{1+tg^2\,\theta_M}\;; \qquad y_o/d = \frac{2\,tg\,\theta_M}{1+tg^2\,\theta_M}\;; \qquad a/d = \frac{tg^2\,\theta_M}{1+tg^2\,\theta_M}\,. \tag{A1-4}$$

We have now to find the second point $P_1 = (x_1, y_1)$ limiting the arc of parabola of interest. Let us call θ_1 the grazing angle of incidence in P_1 and be $\overline{P_oP_1}$ the length of the chord. If w is the width of the beam arriving from the synchrotron, we have:

$$\begin{aligned} &y_1 = y_o + w; \qquad x_1 = (y_1^2/4a) - a; \qquad tg\;\theta_1 = (a/(a+x_1))^{1/2}; \\ &\overline{P_oP_1}^2 = (x_o - x_1)^2 + w^2; \qquad \chi = 2(\theta_M - \theta_1), \end{aligned} \tag{A1-5}$$

where χ is the angle between the rays reflected from P_o and P_1, corresponding to the divergence of the reflected beam. We have written the equations (A1-4) in terms of x_o/d and similar, in order to leave d as a free parameter, the choice of which depends upon the experimental requirements. One can choose, for instance, the angle χ in order to fill the grating or, if the mirror is used after the grating, w becomes the important parameter. In any case the set of the eq. (A1-5) is sufficient to obtain the profile of the parabolic mirror.

APPENDIX II -

As in the Appendix I we restrict our considerations to the upper half plane $y \geq 0$. The foci of the ellipse (Fig. 16) F_1 and F_2, corresponding to the source (electron orbit) and its image (monochromator entrance slit), respectively, lie on the x axis. Let Q and q be the lengths of the major and minor half axis of the ellipse, whose equation is

(AII-1) $$y = \frac{q}{Q}(Q^2 - x^2)^{1/2}.$$

The current point on the ellipse will be denoted by $P = (x, y)$ and the arc of ellipse representing the mirror by $\overset{\frown}{P_1 P_2}$. The incident and the reflected beams are described by two lines through F_1 and F_2, respectively:

(AII-2) $$y = m(x+f) \text{ incident beam}; \quad y = k(x-f) \text{ reflected beam.}$$

with $m = tg\,\alpha$ and $k = tg\,\beta$. The tangent to the ellipse have, in turn, an angular coefficient

(AII-3) $$\ell = tg\,\beta = \frac{dy}{dx} = \frac{-q^2}{Q^2}\frac{x}{y} = -\frac{q}{Q}(x^2/(Q^2-x^2)).$$

Let us make use of the conditions of Section IV. Condition a) gives immediately, from the geometrical definition of an ellipse,

(AII-4) $$Q = \frac{D+d}{2},$$

which, jointly with the relation

(AII-5) $$Q^2 = q^2 + f^2,$$

reduces to one the number of parameters to be determined.

Let us now analyze how the grazing angle of incidence changes with x. From $\theta = \pi + \alpha - \beta$ we have:

(AII-6) $$tg\,\theta = tg(\alpha - \beta) = \frac{m - \ell}{1+m\ell} = \frac{Q\,q}{f(Q^2-x^2)^{1/2}}.$$

We see that $tg\,\theta$ decreases with decreasing $|x|$, having a minimum equal to q/f at x = 0. The condition b) is verified at the point P_2 nearest to the monochromator, so that, from $tg\,\theta|_{P_2} = tg\,\theta_M$, we obtain:

(AII-7) $$x_2 = Q\sqrt{1 - \frac{q^2}{f^2 tg^2\,\theta_M}} = \frac{Q}{tg\,\theta_M}\sqrt{tg^2\,\theta_M - (\frac{Q^2}{f^2} - 1)}$$

$$y_2 = \frac{q^2}{f\,tg\,\theta_M} = \frac{f}{tg\,\theta_M}(\frac{Q^2}{f^2} - 1)$$

The condition of reality of the square root in the first of eq. (AII-7) gives

(AII-8) $$tg^2\,\theta_M \geq \frac{Q^2}{f^2} - 1 > 0.$$

Actually, very small values of θ_M are required, so that $tg^2\,\theta_M \ll 1$ and also $\frac{Q^2}{f^2} - 1 \ll 1$. Let us

put $u^2 = (Q^2/f^2)-1$; this will be the parameter of the ellipse to be determined. We can rewrite equations (AII-3) to (AII-7) as

(AII-9) $$tg\,\beta = -\sqrt{\frac{u^2}{1+u^2}}\sqrt{\frac{x^2}{Q^2-x^2}}$$

(AII-10) $$q = fu$$

(AII-11) $$tg\ \theta = u\sqrt{\frac{Q^2}{Q^2-x^2}}$$

(AII-12) $$x_2 = \frac{Q}{tg\,\theta_M}\sqrt{tg^2\,\theta_M - u^2}$$

(AII-13) $$y_2 = \frac{Q}{tg\,\theta_M}\sqrt{\frac{u^2}{1+u^2}}$$

Writing explicitely the condition a) as

$$(x_1+f)^2 + y_1^2 = D^2; \qquad (x_1-f)^2 + y_1^2 = d^2,$$

the position of P_1 is easily obtained:

(AII-14) $$x_1 = \frac{D-d}{2}(1+u^2)^{1/2}; \qquad y_1 = \frac{1}{2}\sqrt{\frac{u^2}{1+u^2}}\sqrt{4Q^2-(D-d)^2(1+u^2)}$$

So far we have expressed the parameters of the mirror (x_1, y_1, x_2, y_2) in terms of the ellipse's parameters Q and u, but u has yet to be determined. This can be done, for instance, by setting the grazing incidence angle at the point P_1. We make use of the conditions c) and d):

(AII-15) $$\alpha_{P_1} = \alpha_{P_2} + \delta\,; \qquad \alpha'_{P_1} = \alpha'_{P_2} + \chi\,.$$

We have also the following relations between the angles:

(AII-16) $$\theta = \pi + \alpha - \beta\,; \qquad \theta = \beta - \alpha'.$$

After some manipulations we obtain

(AII-17) $$\theta_{P_1} = \theta_M + \frac{\delta-\chi}{2}\,.$$

Passing from the tangents to the angles, from eq. (AII-11) and (AII-14), we find:

(AII-18) $$u^2 = \frac{4Ddtg^2(\theta_M + \frac{\delta-\chi}{2})}{(D+d)^2+(D-d)^2tg^2(\theta_M+\frac{\delta-\chi}{2})}\,.$$

APPENDIX III -

We describe here the focusing and polarization properies of the spherical mirror constructed at the Frascati facility to focus the synchrotron light on the entrance slit of a near-normal incidence monochromator (Fig. 17).

a) Focus. -

The mirror has a radius of curvature of R = 380 cm, a diameter d = 30 cm and a width of 6 cm. It will focus a nearly parallel beam of rays at grazing incidence. The beam is about 35 mm wide, so that the angle of incidence will range from 75° to 80°. The average horizontal and vertical foci are obtained setting $s = \infty$ and $\vartheta_M = 77^{\circ}30'$ in the equation (9) and are $s_h = 38$ cm and $s_v = 880$ cm, respectively. The vertical entrance slit of the monochromator is located at the position of the horizontal focus.

b) Astigmatism. -

The spherical aberration of the mirror will produce a diffuse light spot with a brighter central part. Since the light source is not on the optical axis, it will be focused in a vertical line at the horizontal focus. The length of this astigmatic image (coma) can be calculated from the formula[33]

$$z = \ell\,(1 + 2\sin^2\vartheta) \tag{AIII-1}$$

where ℓ is the vertical lenght of the source. At normal incidence $\vartheta = 0$, $z/\ell = 1$ and the image is stigmatic. The astigmatism becomes severe at grazing incidence. At $\vartheta = 77^{\circ}30'$ an object 1 cm height will be imaged in a line z = 2.90 cm heigh.

c) Polarization. -

The surface of the mirror is covered with a gold film to increase its reflectivity. The reflectance of gold for light polarized parallel (p) or perpendicular (s) to the incidence plane has been calculated in the working range of the monochromator (400 Å - 2000 Å) with the Fresnel formulas, using the optical constant n and k of gold reported by Canfield et al[19] and setting $\vartheta = 78^{\circ}$. If we define the degree of polarization of the light after the reflection as

$$\mathcal{P}_r = \frac{I_{\parallel} R_p - I_{\perp} R_s}{I_{\parallel} R_p + I_{\perp} R_s} \tag{AIII-2}$$

we can calculate $\mathcal{P}_r$ versus λ in both horizontal and vertical mountings. In the latter case, R_p and R_s in the formula (AIII-2) are interchanged. The results are reported in Fig. 20 and compared with the degree of polarization of the incident light reproduced from Fig. 5. We see that the polarization losses in the horizontal mounting never exceed 10% and the gain in the vertical mounting is of the same order of magnitude.

Let us now introduce the effect of the variable angle of incidence due to the finite size of the beam on the reflectively of the mirror. If Σ_0 is the incident energy per unit time and per unit surface normal to the direction of propagation of the beam, the energy reflected at an angle φ for both polarizations is $\Sigma(\varphi) = \Sigma_0 R_{\parallel,\perp}(\varphi)$. The reflectivity of the mirror is therefore

$$\mathcal{R}_{\parallel,\perp} = \int_{\varphi_1}^{\varphi_2} R_{\parallel,\perp}(\varphi)\cos\varphi\, d\varphi \Big/ \int_{\varphi_1}^{\varphi_2} \cos\varphi\, d\varphi \tag{AIII-3}$$

where φ_1 and φ_2 depend on the size of the incident beam. For a beam width of 3.5 cm and a central angle of incidence of 78°, φ_1 and φ_2 can be calculated with the programme listed in Appendix IV and are $\varphi_1 = 76.9^{\circ}$ and $\varphi_2 = 79.2^{\circ}$ respectively. The integrated values $\mathcal{R}_{\parallel}$ and $\mathcal{R}_{\perp}$ are slightly higher than $R_{\parallel}(78)$ and $R_{\perp}(78)$ owing to the larger weight of the reflectivity for angles $\varphi > 78^{\circ}$. The polarization degree $\mathcal{P}_r$ is, instead, unchanged within 1-2°/oo.

The focusing properties of the mirror have been checked experimentally in the visible region by simulating the optical beam of the synchrotron with a light strip approximately 3.5 cm large and 1 cm high. The rays of the beam were made parallel and defined by a proper slit. The incidence angle of the central rays was about $11,5^{\circ}$. The reflected intensity was measured with a photodiode moving in a plane normal to the direction of the reflected beam. The measured parameters s_h and z were (38.2 ± 0.5) and (3.0±0.1)

cm respectively in good agreement with the estimated values. In Table II we summarize the theoretical values of the mirror with the source (synchrotron electron orbit) at s = 750 cm, 3.5 cm wide at different angles of incidence around the central angle. In Appendix IV we list the computer programmes written to calculate the profile and the integrated reflectivity of the mirror.

TABLE II

Horizontal focus s_h and astigmatic length z of the image of a spherical mirror of radius of curvature R = 380 cm for different central θ_c angles of grazing incidence. θ_1 and θ_2 refers to the minimum and maximum angles of incidence in the case of a light 3.5 cm high. All angles are in degrees.

θ_c	θ_1	θ_2	s_h(cm)	Z
10	8.45	11.32	33.0	2.94
11	9.67	12.17	36.0	2.93
12	10.75	13.10	39.5	2.91
13	11.90	14.02	14.7	2.89
14	14.11	15.87	49.1	2.86

APPENDIX IV -

```
C      CALCOLO DI UNO SPECCHIO SFERICO
       DIMENSION X(500),Y(500),BIN(500),XF(500)
     1 READ(5,100)R,XO,TT,FAS,YTS,YTI,DX,DXF,DYT
       IF(R.LT.0.0001) CALL EXIT
       RR=3.141593/180.
    20 AMM=TAN(FAS/XO)
       TETA=TAN(TT*RR)**2
       ALFA=XO-R*SQRT(TETA/(1.+TETA))
       BETA=-SQRT(R*R-(XO-ALFA)**2)
       A=AMM*AMM+1.
       B=ALFA+AMM*BETA
       C=ALFA*ALFA+BETA*BETA-R*R
       RAD=B*B-A*C
       IF(RAD.LT.0.) GO TO 10
       XA=(B-SQRT(RAD))/A
       XB=(B+SQRT(RAD))/A
       IF(XA-XB) 2,3,3
     2 X1=AINT(XB)
       GO TO 4
     3 X1=AINT(XA)
     4 X2=XO+20.
       N=INT((X2-X1)/DX)+1
       YT=YTS
     8 X(1)=X1
       DO 15 I=1,N
       RQ=SQRT(R*R-(X(I)-ALFA)*(X(I)-ALFA))
       Y(I)=BETA+RQ
       TIN=Y(I)/X(I)
       TB=(ALFA-X(I))/(Y(I)-BETA)
       TA=DOT(TIN,TB,-1.)
       TANIF=DOT(TB,TA,-1.)
       BIN(I)=ATAN(TA)/RR
       XF(I)=X(I)+(YT-Y(I))/TRIF
       M=I+1
       X(M)=X(I)+DX
    15 CONTINUE
       IF(YT.LE.YTI) GO TO 18
       WRITE(6,260) YT
       WRITE(6,225) XO,TT,FAS
       WRITE(6,226)    R,ALFA,BETA
       WRITE(6,270)
       WRITE(6,200) ((X(I),Y(I),XF(I),BIN(I)),I=1,N)
    18 CALL COUNT(N,X,Y,XF,BIN,YT,DXF)
       YT=YT-DYT
       IF(YT.LT.YTI) GO TO 1
       GO TO 8
    10 WRITE(6,230)
       WRITE(6,225) XO,TT,FAS
       WRITE(6,226)    R,ALFA,BETA
       FAS=FAS-1.
       GO TO 20
   100 FORMAT(6F10.0,3F5.0)
   200 FORMAT(F30.2,3F30.5)
   225 FORMAT(///,15H PARAMETRI DATI,10X,5HSP-SR,F7.1,10X,6HAN INC,F7.0,1    225 1
     10X,6HLAR FS,F7.1,//)                                                  225 2
   226 FORMAT(//,16H ALTRI PARAMETRI,10X,6HRAGGIO,F7.1,10X,4HALFA,F10.3,1
     10X,4HBETA,F10.3)
   230 FORMAT(1H1,///,21H CALCOLO NON ESEGUITO,//)
   260 FORMAT(1H1,//,43X,39HFOGHEGGIAMENTO SPECCHIO SFERICO PER Y=,F5.1,//
     1/)
   270 FORMAT(//,20X,10HX SPECCHIO,20X,10HYSPECCHIO,20X,10HX IMMAGINE,20X
     1,10HANGOLO INC,/)
       END
```

```
@FOR,IS COUNT
      SUBROUTINE COUNT(N,X,Y,XF,BIN,YT,DXF)
      DIMENSION XF(500),Y(500),X(500),INDEX(500),BIN(500)
      WRITE(6,260) YT
      CALL EXTR(N,XF,XFS,XFI)
      XA=XFI
   10 XB=XA+DXF
      DO 5 I=1,N
    5 INDEX(I)=0
      NUM=0
      M=1
      DO 1 I=1,N
      IF(XF(I).GT.XA.AND.XF(I).LE.XB) GO TO 2
      GO TO 1
    2 NUM=NUM+1
      INDEX(M)=I
      M=M+1
    1 CONTINUE
      IF(NUM.LT.10) GO TO 4
      WRITE(6,222) XA,XB,NUM
      WRITE(6,270)
      K=1
      DO 3 I=1,N
      IF(INDEX(K).NE.I) GO TO 3
      K=K+1
      WRITE(6,200) X(I),Y(I),XF(I),BIN(I)
    3 CONTINUE
    4 XA=XB
      IF(XA.NE.XFS) GO TO 10
  260 FORMAT(1H1,//,43X,39HFOCHEGGIAMENTO SPECCHIO SFERICO PER Y=,F5.1,//
     1/)
  222 FORMAT(//,36H PUNTI FOCHEGGIATI NELL-INTERVALLO (,F9.1,2H ,,F9.1,2   222 1
     1H ),I10)
  270 FORMAT(//,20X,10HX SPECCHIO,20X,10HYSPECCHIO,20X,10HX IMMAGINE,20X
     1,10HANGOLO INC,/)
  200 FORMAT(F30.2,3F30.5)
      RETURN
      END
@FOR,IS TTT
      FUNCTION DDT(A,B,E)
      DDT=(A+E*B)/(1.-E*A*B)
      RETURN
      END
@FOR,IS EXTR
      SUBROUTINE EXTR(N,X,Y,Z)
      DIMENSION X(500)
      Y=X(1)
      Z=X(1)
      DO 1 I=1,N
      IF(X(I).GT.Y) Y=X(I)
    1 IF(X(I).LT.Z) Z=X(I)
      Y=AINT(Y)+1.
      Z=AINT(Z)-1.
      RETURN
      END
C PROGRAMMA PER IL CALCOLO DELLA RIFLETTIVITA' INTEGRATA SULL'ANGOLO
C
      READ(5,10) F1,F2
      F1=F1/57.29578
      F2=F2/57.29578
      DF=(F2-F1)/20.
      PRINT 26
 26   FORMAT(1H1,5X,'LAMBDA',,5X,'PERP',5X,'PARALL',,//)
25    READ(5,11) AL,AN,AK
10    FORMAT(2F10.0)
11    FORMAT(3F10.0)
      IF(AN.LT..00001) CALL EXIT
      F=F1
      SUM1=.0
```

```
      SUM2=.0
22    FAT=.5
21    CALL REFL(AN,AK,F,RP,RS)
      SUM1=SUM1+RS*FAT*COS(F)
      SUM2=SUM2+RP*FAT*COS(F)
      F=F+DF
      FAT=1.
      IF(F-F2) 21,22,23
23    SUM1=SUM1*DF/(SIN(F2)-SIN(F1))
      SUM2=SUM2*DF/(SIN(F2)-SIN(F1))
      PRINT 24,AL,SUM1,SUM2
24    FORMAT(2X,3F10.3)
      GO TO 25
      END
$FOR,IS REFL
      SUBROUTINE REFL(AN,AK,F,RP,RS)
C  CALCOLA LA COMPONENTE PARALLELA(RP) E PERPENDICOLARE(RS) DELLA RIFLETTIVITA'
      COM=AN*AN-AK*AK-SIN(F)**2
      A=SQRT(.5*(SQRT(COM**2+4.*AN*AN*AK*AK)+COM))
      B=SQRT(.5*(SQRT(COM**2+4.*AN*AN*AK*AK)-COM))
      TOT=A*A+B*B+COS(F)**2
      RS=(TOT-2.*A*COS(F))/(TOT+2.*A*COS(F))
      DAT=A*A+B*B+SIN(F)**2*TAN(F)**2
      RP=RS*(DAT-2.*A*SIN(F)*TAN(F))/(DAT+2.*A*SIN(F)*TAN(F))
      RETURN
      END
```

REFERENCES -

(1) - We will call hereafter "vacuum ultraviolet (VUV)" the spectral region extending roughly from 2000 Å to 2 Å, which usually is divided into the far ultraviolet range (FUV) down to 400 Å, and soft x--rays at shorter wavelengths.
(2) - Frascati, Synchrotron radiation facility and experimental results, CERN Courrier 4, 42 (1972).
(3) - Synchrotron radiation facilities, CERN Courrier 4, 130 (1972).
(4) - D.H. Tomboulian, Cornell Univ. Rep. NP 5803 (1955); Y. Cauchois, Mem. Soc. Roy. Sci. Liège 1, 105 (1971); Y. Cauchois, C. Bonnelle and G. Missoni, Compt. Rend. 257, 409 (1963); M.U. Meyer--Berkhout, DESY Report, NP 16354 (1966); T. Oshio and T. Sagawa, Rigaku-Denki Janaru 7, 12 (1965);R.P. Madden, D.L. Ederer and K. Codling, Appl. Opt. 6, 31 (1967);C.H. Pruett, E. M. Rowe, R.A. Otte and J.D. Steben, Bull. Am. Phys. Soc. 14, 17 (1969); G.V. Marr and I.H. Munro, New Sci. J. 49, 266 (1971).
(5) - R.P. Godwin, Springer Tracts in Modern Physics (Berlin Springer, 1969), vol. 51.
(6) - W. Hayes, Contemp. Phys. 13, 441 (1972).
(7) - J.A.R. Samson, Techniques of Vacuum Ultraviolet Spectroscopy, (John Wiley and Sons, New York 1967).
(8) - A.N. Zaidel' and E. Ya. Shreider, Vacuum Ultraviolet Spectroscopy, (Ann. Arbor, London 1970).
(9) - J. Schwinger, Phys. Rev. 75, 1912 (1949).
(10) - A.A. Sokolov and J.M. Ternov, Synchrotron Radiation, (Pergamon Press, Oxford, 1968).
(11) - P.L. Hartman and D.H. Tomboulian, Phys. Rev. 91, 1577 (1953); D.H. Tomboulian and P.L. Harman, Phys. Rev. 102, 1423 (1956); D.H. Tomboulian and D.E. Bedo, J. Appl. Phys. 29, 804 (1958).
(12) - K. Codling and R.P. Madden, J. Appl. Phys. 36, 380 (1965).
(13) - G. Missoni and A. Ruggiero, Atti Acc. Naz. Lincei, Rend. Cl. Sci. Fis. Mat. Nat. 38, 677 (1965).
(14) - A. Balzarotti, M. Piacentini and M. Grandolfo, Lett. Nuovo Cimento 3, 15 (1970).
(15) - A. Balzarotti, L. Bartolini, A. Bianconi, E. Burattini, M. Grandolfo, R. Habel, M. Piacentini, Frascati Report, LNF-72/98 (1972).
(16) - The path of 1 cm roughly corresponds to the portion of orbit observed from the experimental area, as shown in the next paragraph.
(17) - Only one solution exists in the upper half plane if D > R.
(18) - We found very useful the Kodak Linograph Direct Print Paper used in recorders working with small uv radiation pens. Such a paper is not sensitive to the visible spectrum and it does not need to be developed.
(19) - L.R. Canfield, G. Hass and W.R. Hunter, J. de Physique 25, 154 (1964).
(20) - G. Hass and R. Tousey, J. Opt. Soc. Am., 49, 593 (1959).
(21) - W.R. Hunter, Optica Acta 9, 255 (1962).
(22) - C. Kunz, Proc. Int. Symp. for Sunchrotron Radiation Users (Daresbury 1973); M. Piacentini and G. Strinati, Frascati Report LNF 73/38 (1973).
(23) - R.J. Speer and D. Turner, Proc. Intern. Symp. for Synchrotron Radiation Users (Daresbury 1973), pag. 106.
(24) - W.R. Hunter, D.W. Angel and R. Tousey, Appl. Opt. 4, 891 (1965).
(25) - K. Codling, R.P. Madden, W.R. Hunter and D.W. Angel, J. Opt. Soc. Am. 56, 189 (1966).
(26) - J.A. Samson and R.B. Cairns, Appl. Opt. 4, 915 (1965).
(27) - T. Sasaki and M. Inokuti, 3rd Int. Conf. on Vacuum Ultraviolet Rad. Physics, (Phys. Soc. Japan, Tokyo 1971).
(28) - G. Sprague, D.H. Tomboulian and D.E. Bedo, J. Opt. Soc. Am. 45, 756 (1955).
(29) - S. Fujiwara and Y. Iguchu, J. Opt. Soc. Am. 58, 1189 (1968).
(30) - While the discussion given in the preceeding Sections was completely general, the problems connected with the measurements are specialized changing with each kind of experiment. Therefore in this Section we shall restrict ourself only to reflection and transmission experiments on solids; nevertheless several topics discussed below hold also for other kinds of experiments.
(31) - Very popular are the Bendix electron multipliers,both the magnetic types and the channeltron types.
(32) - M.R. Howells and L. Naylor, DNPL Reports TM 98 (1972).
(33) - H.G. Bentler, J. Opt. Soc. Am. 35, 311 (1945); T. Namioka, J. Opt. Soc. Am. 49, 446 (1959); 51, 4 (1961).